universität
innsbruck

Bachelor thesis

A beam splitter for interacting quantum particles

Ing. Mathias Andreas Schöpf

30th July 2023

Supervised by Dr. Laurin Ostermann
and Univ.-Prof. Mag. Dr. Helmut Ritsch
Institute for Theoretical Physics

Statutory declaration

I hereby declare in lieu of an oath with my own handwritten signature that I have written this thesis independently and have not used any sources or aids other than those specified. All passages that have been taken from the specified sources, either verbatim or in terms of content, are marked as such.
I agree to the archiving of this bachelor thesis.

Innsbruck, on 30th July 2023   Ing. Mathias Andreas Schöpf

Abstract

This thesis investigates the possibility of numerically simulating a beam splitter for ultracold atoms using tunneling through a potential barrier. The theory chapters cover the basic concepts of the topics required (quantum gases, Gross-Pitaevskii equation, tunnel effect) to understand the physical principles underlying the numerical simulations done in Julia with the QuantumOptics.jl toolbox. This is complemented by a description of this toolbox and the methods used for numerical calculation.
First, we numerically exhibit the basic idea of splitting an incoming wavepacket. The effect of the pseudopotential was demonstrated, as well as the heavy particle approximation. We show that the effect of the interaction is small for suitable parameters. A comparison between the soliton solutions and a Gaussian wave package didn't result in visually observable differences. Changing the width of the potential changed the shape and offset of the reflected wave and the law of reflection could also be shown to hold true for a BEC.
However, there were also some issues that prevent the simulation of an interferometer with this contraption. The most critical one being the inability to have a non-expanding wave after the split at the barrier due to the limited range of the g-Factor.

Contents

1 Introduction

Ever since the discovery of matter waves and consequentially of quantum theory, a considerable amount of time and resources have been invested in experiments and theoretical models to describe the behavior of such waves. Many phenomena from optics have been reproduced with matter waves (like interference), while other phenomena are completely unique to matter waves (e.g. dipolar quantum gases).

One of the phenomena that was recently experimentally reproduced is the so-called beam splitting [2]. This is essential for interferometers. In optics, you would usually have a laser that shines on a semi-reflective mirror with a refractive index that is just big enough for 50% of the light to transmit through the material and 50% of the beam to reflect from the mirror (see fig. 1.1). All that is really required for this to work is a material with the desired refractive index, so this is very easy to manufacture. However, this does not work with matter waves. If you would launch a matter wave (e.g. an electron) onto any material, all you would likely get is Rutherford scattering. In most cases, the particle would just get absorbed by the material. Direct reflections are

Figure 1.1: A beam typical beam splitter in optics. In this case, the semi-reflective material is provided by a coating for phase consistency of the wave. [1]

very rare because the particle would have to directly hit the center of an atom to get reflected. Therefore one cannot get a similar behavior of matter waves with a solid semi-reflective mirror. But instead of a material that reflects the particle one could create a potential barrier and utilize the tunnel effect for reflection and transmission. But we are facing an issue here with matter waves: Due to Heisenberg's uncertainty principle, regular matter waves will naturally disperse, so we won't have a point like beam hitting the "mirror", but rather a broad wave front that continues to disperse after the potential barrier. This makes building an interferometer technically challenging. So to prevent this, one could use a Bose-Einstein condensate (in short BEC) instead of thermal atoms. The BEC has a self-interaction term that can prevent the dispersion of the wave function. Therefore the goal of this thesis is to analyze the feasibility of a beam splitter using a BEC and a potential barrier. This could then be used to build a matter wave interferometer if the technical challenges can be overcome.
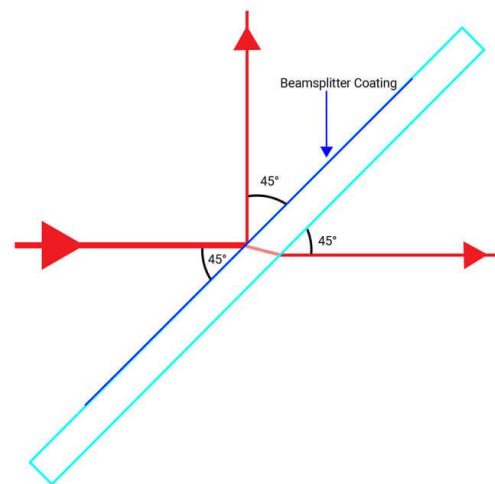
2 Theory

2.1 Quantum gases

Quantum gases are one of the most fundamental topics in quantum physics. Their roots go back to the very first discovery of quantum effects (Planck's law of radiation, coming from the study of photon gases), even though at that time it wasn't clear where those effects come from. Together with various other areas of research, this eventually lead to the development of quantum theory. Today, many areas of research are based on quantum gases, ranging from fundamental research on complicated forms of quantum gases (such as molecular quantum gases) to solid-state physics and condensed matter physics (e.g. in figure 2.1), to the study of gases within gas giants and stars.

As we can already see, quantum gases are very important in modern physics in general, but also for this thesis. This section, therefore, covers the very basics of quantum gases in order to gain a sufficient understanding of the topic for the rest of this thesis. However, a closer look at quantum gases is recommended to fully understand the topic and can be usually found in any book on statistical physics. The book used for this thesis (in German) is given in reference [3].

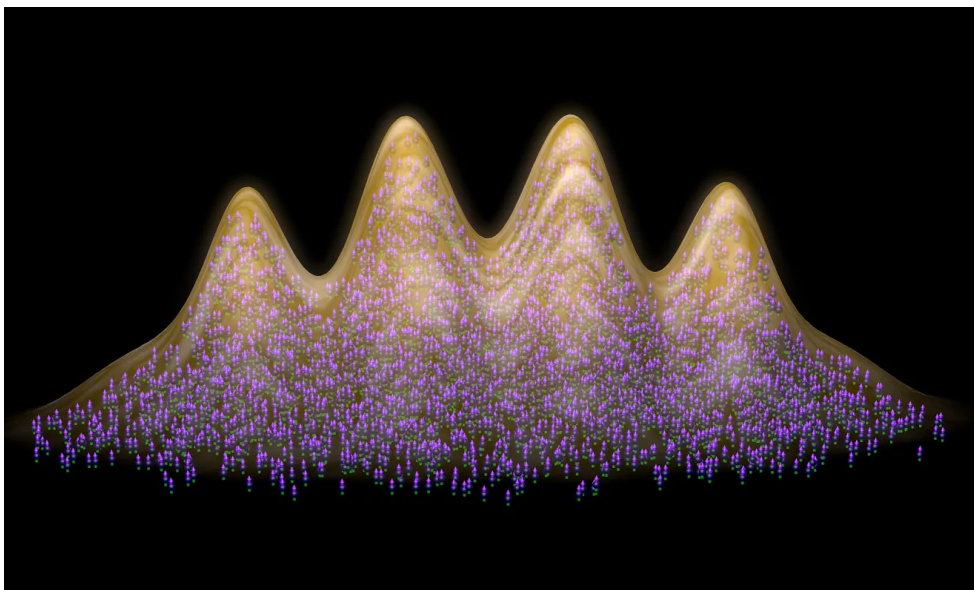**Figure 2.1:** *Researchers led by Francesca Ferlaino at the University of Innsbruck and Austrian Academy of Sciences report in Physical Review X on the observation of supersolid behavior in* **dipolar quantum gases** *of erbium and dysprosium. In the dysprosium gas these properties are unprecedentedly long-lived. This sets the stage for future investigations into the nature of this exotic phase of matter.* [4]

2.1.1 Quantum gases in general

The basic description of quantum gases sounds quite straightforward: Quantum gases differ from regular gases by the dominance of quantum effects related to their wave nature and symmetry constraints. So those can be spin-spin interactions, state occupations, etc. Thermal movement usually weakens those effects and turns the quantum gas into a regular gas, therefore most quantum gases have to be cooled to a temperature near absolute zero. Very rarely, some quantum gases can be described at fairly high temperatures (electron gas approximation in a conductor for example). Some quantum gases have even been shown to form far above the theoretical predictions for their maximum temperature and are thus in active research (high-temperature superconductors come to mind).

Between the regular gaseous state and the quantum gas state, all quantum gases go through a phase transition where either quantum effects or thermal effects become dominant, depending on the direction of the temperature change. At the exact temperature of the phase transition, both effects are equally strong, thus forming a mixed state similar to e.g. ice water.

Since there are only two fundamental particle types in quantum theory, there are also just two fundamental quantum gases in statistical physics:

- Fermi gas: As the name suggests, this is a gas consisting of fermions, i.e. particles with half-integer spin, obeying Fermi-Dirac statistics.

- Bose-Einstein condensate: Again derivable from the name, this is a gas consisting of bosons, i.e. particles with integer spin, which is governed by Bose-Einstein statistics.

These form the very basis of quantum gases. Many complicated problems use one of these gases as an approximation for the real system in order to get a quick result and then introduce modifications to the gas to get a better approximation for the problem (e.g. the free electron approximation in solid state physics).

2.1.2 Bose-Einstein condensate

As already mentioned, the Bose-Einstein condensate (in short BEC) is a gas made of bosons. Bosons are integer spin particles, which means they don't follow the Pauli exclusion principle. Fermions, on the other hand, being half-integer spin particles, do follow the exclusion principle. As a reminder, the Pauli exclusion principle states that two half-integer spin particles cannot occupy the same state. This has a major impact on the behavior of the gas.

But first, we have to get a certain sense of what temperature actually means for our gases as they approach temperatures near absolute zero. An imprecise, but sufficient description of temperature for this thesis is as a measurement of energy, usually connected by the Boltzmann constant like $E = k_\mathrm{B}T$. The most important part here is when the temperature approaches zero, the energy reaches its minimum. Quantum mechanically speaking this means that the gas has to be in the lowest possible energy state.

What does that mean for our two gases? Let's imagine we have a box that we fill with bosons. Each boson is cooled to $0\,\mathrm{K}$. Now we add the first boson. The lowest possible energy state in our system is the ground state. Therefore as the boson cools down, it will occupy the

ground state. If we then add a second boson, it will also occupy the ground state, because bosons don't follow the Pauli principle and can therefore occupy the same state multiple times. So all bosons that we add to this box will occupy the ground state.

Now let's do the same with fermions. We add the first fermion, which again will occupy the ground state. But if we add a second fermion, it cannot occupy the ground state since the ground state is already taken by the first fermion. Therefore the second fermion has to occupy the next higher state. So as we add fermions to the box, we will fill up all the lowest possible states up to a certain energy called the fermi energy.

This difference is illustrated in figure 2.2. The upper picture shows all bosons occupying the lowest possible state, so the ground state. The fermions can only occupy each state once and therefore fill up the lowest states up to the fermi energy E_F.

This has many implications for the BEC, two of the most famous ones probably being superconductivity and superfluidity. But the focus of this thesis is not so much on the statistical physics of the gas, but rather on the wave mechanics of the gas. Since all bosons are in the same state (the ground state), all bosons share the same wave function. Due to weak attractive forces between the bosons, the particles will start to gather on a single point. As these particles

Figure 2.2: Comparison of bose gases (BECs) and fermi gases. [5]

move closer together, their wave functions will start to overlap and form a single wave function that can be used to describe the gas as a whole. This creation process of a BEC, as it cools down, is illustrated in figure 2.3 (starting on the left and moving to the right).
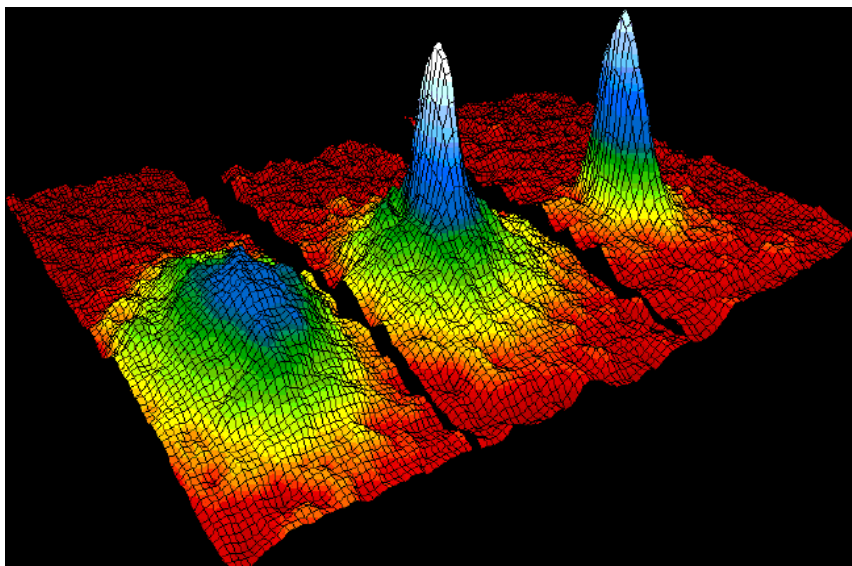
Figure 2.3: *Velocity-distribution data (3 views) for a gas of rubidium atoms, confirming the discovery of a new phase of matter, the Bose–Einstein condensate. Left: just before the appearance of a Bose–Einstein condensate. Center: just after the appearance of the condensate. Right: after further evaporation, leaving a sample of nearly pure condensate.* [6]

2.2 Gross-Pitaevskii equation

Bose-Einstein condensates require a different treatment than single quantum particles due to their self-interactions. This can be effectively described via a nonlinear self-interaction term in the Schrödinger equation. The resulting equation is then called the nonlinear Schrödinger equation or more commonly Gross-Pitaevskii equation. This section focuses on the derivation of the equation as well as some possible solutions and approximations.

2.2.1 Derivation of the equation

The following derivation was heavily inspired by [7]. More information on the GPE can be found in reference [8].

As already mentioned, the BEC interacts with itself, which comes from a weak potential between each particle in the BEC. A general ansatz for a Hamiltonian that considers this would be:

$$H = \sum_i \left(-\frac{\hbar^2}{2m}\nabla_i^2 + U(\boldsymbol{r}_i) \right) + \frac{1}{2}\sum_{i \neq j} V(\boldsymbol{r}_i - \boldsymbol{r}_j) \tag{2.1}$$

Since each interaction is summed over twice, we have to half the sum over all particle potentials. This can then be inserted into the time-dependent Schrödinger equation using an ansatz $\psi(\boldsymbol{r}_1, \boldsymbol{r}_2, ..., \boldsymbol{r}_N, t)$ for the many-body system:

$$i\hbar\frac{\partial}{\partial t}\psi(\boldsymbol{r}_1, \boldsymbol{r}_2, ..., \boldsymbol{r}_N, t) = H\psi(\boldsymbol{r}_1, \boldsymbol{r}_2, ..., \boldsymbol{r}_N, t) \tag{2.2}$$

We can then apply the variational principle onto equation 2.2, which leads to the following functional:

$$S = \int_\Omega \psi^\dagger \left(i\hbar\frac{\partial}{\partial t} - H \right) \psi \, \mathrm{d}t \, \mathrm{d}^3\boldsymbol{r}_1 \, \mathrm{d}^3\boldsymbol{r}_2 \, ... \, \mathrm{d}^3\boldsymbol{r}_N \tag{2.3}$$

Next, we assume that the gas has a temperature of absolute zero and therefore, as described in section 2.1.2, all particles occupy the same state. This allows us to apply the Hartree-Fock approximation, which means that we assume that the wave function can be constructed by products of single-particle wave functions:

$$\psi(\boldsymbol{r}_1, \boldsymbol{r}_2, ..., \boldsymbol{r}_N, t) = \prod_i \psi_i(\boldsymbol{r}_i, t) \tag{2.4}$$

Inserting this back into our functional in equation 2.3, we get:

$$S = \int_\Omega \psi(\boldsymbol{r}, t)^\dagger \left(i\hbar\frac{\partial}{\partial t} + \frac{\hbar^2}{2m}\nabla^2 - U(\boldsymbol{r}) - (N-1)\int_\Omega |\psi(\boldsymbol{r}', t)|^2 V(\boldsymbol{r}' - \boldsymbol{r}) \, \mathrm{d}^3\boldsymbol{r}' \right) \psi(\boldsymbol{r}, t) \, \mathrm{d}t \, \mathrm{d}^3\boldsymbol{r} \tag{2.5}$$

The rewriting of the potential was possible since each integral over the potential will always yield the same result, therefore we can rewrite the sum over each particle in equation 2.1 into the number of particles times the potential. The second integral and the absolute squared of the wave function comes from the recombination of the outer integrals into one integral.

This can then again be re-substituted into equation 2.2, which leads to:

$$i\hbar\frac{\partial}{\partial t}\psi(\boldsymbol{r}, t) = \left(-\frac{\hbar^2}{2m}\nabla^2 + U(\boldsymbol{r}) + (N-1)\int_\Omega |\psi(\boldsymbol{r}', t)|^2 V(\boldsymbol{r}' - \boldsymbol{r}) \, \mathrm{d}^3\boldsymbol{r}' \right) \psi(\boldsymbol{r}, t) \tag{2.6}$$

After that, we assume a dilute gas and use a Fermi pseudopotential $V(\boldsymbol{r}) = \frac{4\pi\hbar^2 a_{\mathrm{S}}}{m}\delta(\boldsymbol{r})$, which utilizes 3D wave scattering theory. Since integrating a Dirac delta distribution [9] times a function $\delta(\boldsymbol{r}' - \boldsymbol{r})f(\boldsymbol{r}')$ over $\boldsymbol{r}'$ yields the function at point $\boldsymbol{r}$,

$$\int_\Omega \delta(\boldsymbol{r}' - \boldsymbol{r})f(\boldsymbol{r})\,\mathrm{d}\boldsymbol{r}' = f(\boldsymbol{r}) \tag{2.7}$$

we then finally get our Gross-Pitaevskii equation:

$$i\hbar\frac{\partial}{\partial t}\psi(\boldsymbol{r}, t) = \left(-\frac{\hbar^2}{2m}\nabla^2 + U(\boldsymbol{r}) + (N-1)\frac{4\pi\hbar^2 a_{\mathrm{S}}}{m}|\psi(\boldsymbol{r}, t)|^2\right)\psi(\boldsymbol{r}, t) \tag{2.8}$$

The factor before the absolute squared is then usually substituted by a constant g, which then leads to:

$$i\hbar\frac{\partial}{\partial t}\psi(\boldsymbol{r}, t) = \left(-\frac{\hbar^2}{2m}\nabla^2 + U(\boldsymbol{r}) + g|\psi(\boldsymbol{r}, t)|^2\right)\psi(\boldsymbol{r}, t) \tag{2.9}$$

The only difference to the regular time-dependent Schrödinger equation now being the pseudopotential $V_{\mathrm{pseudo}} = g|\psi(\boldsymbol{r}, t)|^2$. We can now also see why the Gross-Pitaevskii equation is often called nonlinear Schrödinger equation: The pseudopotential contains a nonlinear dependency on the wave function, making the whole equation nonlinear.

2.2.2 Solitons

Solitons (or solitary waves) describe a wave packet that, due to the cancellation of dispersive effects, maintains its shape. Their definition, according to [10], is:

- Their partial shape is constant in time;

- They are localized within a region;

- They can interact with other solitons, and emerge from the collision unchanged, except for a phase shift.

The first solitary wave was described for water waves by John Scott Russell in 1834 on the Edinburgh-Glasgow canal, which he called the "great wave of translation". [10]
Due to the pseudopotential derived in section 2.2.1 and described in chapter 1, the BEC counters its natural dispersive behavior and therefore maintains its shape. It can also interact with other solitons and emerge unchanged. BECs thus fulfill the definition of solitons. Again, as mentioned in chapter 1, this is crucial for building an interferometer. Otherwise, the particles would just continually disperse and change their form within the potential, creating multiple problems.

2.2.3 Typical models for solitons

Two models for solitons are often differentiated: The bright soliton solution with a positive amplitude (see figure 2.4) and the dark soliton solution with a negative amplitude (see figure 2.5). In addition to this, gaussian wave packages (see figure 2.6) are often used as an approximation which still yields good results.
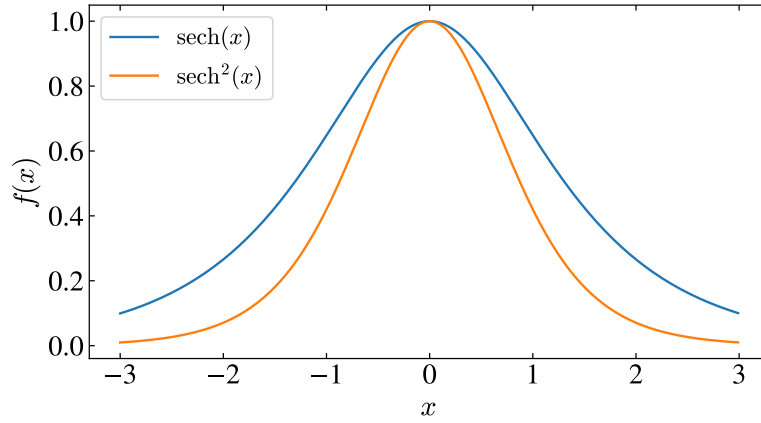
Bright soliton solution

Figure 2.4: The general form of the bright soliton solution (blue) and its probability density (orange).

The bright soliton solution in 1D is based on the $\text{sech}(x)$ function (the inverse of $\cosh(x)$) with the following coefficients (see [11] for reference):

$$\psi(x) = \sqrt{\frac{m|g|}{8\hbar^2}} \,\text{sech}\left(\frac{m|g|}{4\hbar^2}x\right) \tag{2.10}$$

with mass m and the proportionality factor g of the pseudopotential.

Dark soliton solution
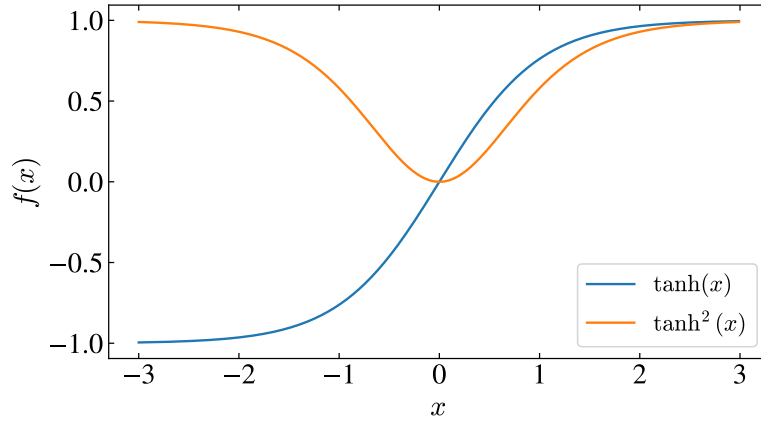
Figure 2.5: The general form of the dark soliton solution (blue) and its probability density (orange).

An analogues ansatz can be made for the dark soliton solution, which is based on the $\tanh(x)$ (see [11] for reference):

$$\psi(x) = \bar{\psi} \tanh\left(\sqrt{\frac{mg}{\hbar^2}}\bar{\psi}x\right) \tag{2.11}$$

with mass m and the proportionality factor g of the pseudopotential. The factor $\bar{\psi}$ is the value of the wave $\psi(x)$ at $x \to \infty$.

Gaussian particle approximation
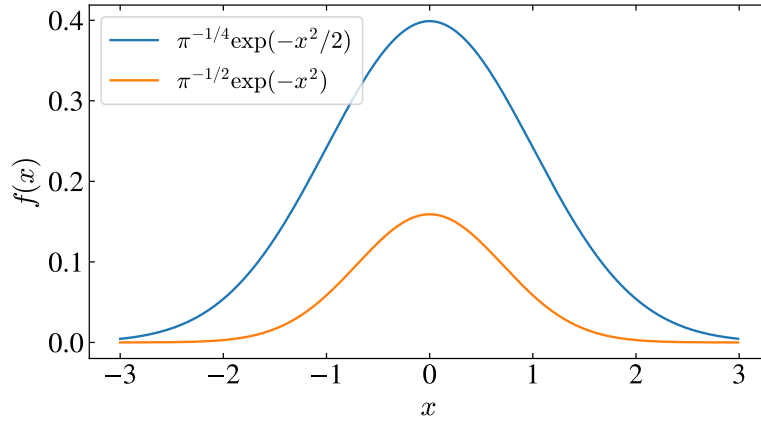
Figure 2.6: The general form of the dark soliton solution (blue) and its probability density (orange).

An approximation to both solutions can be made with Gaussian particles, which are given by a regular Gaussian distribution:

$$\psi(x) = \left(\frac{1}{\pi\sigma^2}\right)^{1/4} \exp\left(-\frac{x^2}{2\sigma^2}\right) \tag{2.12}$$

with σ determining the width of the wave function.

2.2.4 Effect of the pseudopotential
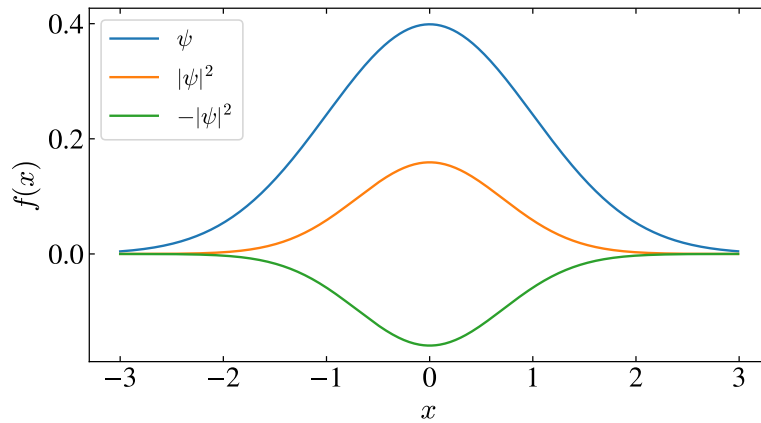
Figure 2.7: A comparison of attractive (in green) and repulsive (in orange) potentials for a Gaussian wave (in blue).

The pseudopotential can have different effects on the BEC depending on the proportionality factor g as can be seen in figure 2.7. For $g > 0$, the potential will be repulsive and thus increase the natural dispersion of the wave. For $g < 0$, the potential will be attractive and therefore decrease or even eliminate the natural dispersion of the wave.

2.3 Heavy particle approximation

Gaussian wave packages disperse over time. This is due to their dispersion relation. But the time it takes for the particle to increase in size depends on its mass. The following section will derive this relation and explain its relevance to our problem. The whole derivation can be found in [12].

If we start with a Gaussian wave package in momentum space

$$\psi(k) = \frac{\sigma}{2\sqrt{\pi}} \exp\left(-\frac{\sigma^2(k-k_\mathrm{c})^2}{2}\right) \exp(ix_0(k-k_\mathrm{c})) \tag{2.13}$$

and do the inverse Fourier transform for a Taylor expansion of the dispersion relation

$$\omega(k) = k_\mathrm{c}v_\mathrm{p} + (k-k_\mathrm{c})v_\mathrm{g} + (k-k_\mathrm{c})^2\Gamma/2 + ... \tag{2.14}$$

with the coefficients of the Taylor expansion being phase velocity $v_\mathrm{p} = \omega(k_\mathrm{c})/k_\mathrm{c}$, group velocity $v_\mathrm{g} = \omega'(k_\mathrm{c})$ and $\Gamma = \omega''(k_\mathrm{c})$, over $i(kx - \omega(k)t)$ like

$$\psi(x,t) = \frac{\sigma}{2\sqrt{\pi}} \int \exp(i(kx - \omega(k)t)) \exp\left(-\frac{\sigma^2(k-k_\mathrm{c})^2}{2}\right) \exp(ix_0(k-k_\mathrm{c})) \, \mathrm{d}k \tag{2.15}$$

we get a new Gaussian wave function that now has a standard deviation that depends on the time t

$$\psi(x,t) = \exp\left(-\frac{1}{2}\frac{(x-(x_0+v_\mathrm{g}t))^2}{\sigma^2 - i\Gamma t}\right) \exp(ik_\mathrm{c}x) \exp(-ik_\mathrm{c}t(v_\mathrm{g}-v_\mathrm{p})) \tag{2.16}$$

The probability density is then given by

$$|\psi(x,t)|^2 = \exp\left(-\frac{\sigma^2(x-(x_0+v_\mathrm{g}t))^2}{\sigma^4 + \Gamma^2 t^2}\right) \tag{2.17}$$

The standard deviation for this probability density can then be derived as

$$\sigma(t) = \sqrt{\frac{\sigma^4 + \Gamma^2 t^2}{\sigma^2}} \tag{2.18}$$

For non-relativistic particles, the dispersion relation is $\omega(k) = \frac{\hbar k^2}{2m}$. Therefore we get $\omega''(k_\mathrm{c}) = \Gamma = \frac{\hbar}{m}$, which means a higher mass leads to slower expansion of the probability density. This can be used as an approximation for the GPE in case the time frame of the expansion is small enough.
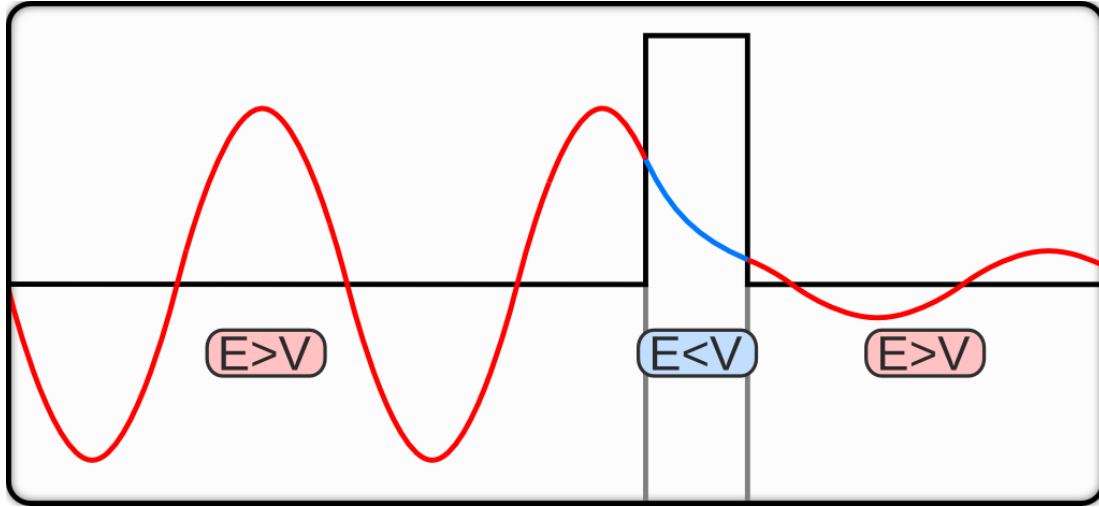
2.4 Tunnel effect

Figure 2.8: Tunnel effect for a stationary elementary wave. [13]

The tunnel effect is a phenomenon of quantum mechanics. In classical physics, a particle cannot pass a potential barrier if its kinetic energy is not larger than the potential. In quantum mechanics, this is indeed possible with a certain probability. In order to describe this, we start with the stationary Schrödinger equation:

$$E\psi = -\frac{\hbar^2}{2m}\nabla^2\psi + V_{\mathrm{B}}\psi \tag{2.19}$$

The solution for this if $V_{\mathrm{B}} < E$ is based on $\cos(x)$ and $\sin(x)$ functions, usually represented by their exponential notation

$$\psi = A\exp(ikx) + B\exp(-ikx) \tag{2.20}$$

where $k = \sqrt{2m(E - V_{\mathrm{B}})}/\hbar$ is the wave vector of the particle. However, if $V_{\mathrm{B}} > E$, then we get exponentially decaying/increasing functions

$$\psi = C\exp(\kappa x) + D\exp(-\kappa x) \tag{2.21}$$

where $\kappa = \sqrt{2m(V_{\mathrm{B}} - E)}/\hbar$ is the decay constant.

This exponential decay leads to a usually small probability that the particle does indeed pass the potential barrier despite having not enough energy, as can be seen in figure 2.8. The wave comes from the left as a free particle, then hits the potential barrier and starts to decay to a certain amplitude. After passing the potential barrier, it continues at a lower amplitude due to the boundary conditions placed on the wave to be continuous.

The reflection that also occurs appears as a modulation of the wave on the left of the potential since the incoming and the reflected wave will overlap here.

This can then be used to split the wave 50:50 if the strength and the width of the potential are tuned to allow that.

3 Simulation Methods

To simulate the Gross-Pitaevskii equation for a Bose-Einstein-Condensate, numerical methods are required due to the nonlinearity of the equation. Therefore, a framework for numerical calculations called QuantumOptics.jl was used to propagate the wave function. It utilized the split-operator method for this simulation. The framework itself and the numerical method are introduced in the following sections.

## 3.1 Introduction to QuantumOptics.jl

Figure 3.1: Logo of QuantumOptics.jl taken from the homepage. [14]

QuantumOptics.jl (in short QO.jl) is a toolbox for the simulation of quantum systems, written in Julia. It was developed by the CQED group led by Univ.-Prof. Mag. Dr. Helmut Ritsch at the University of Innsbruck. The framework was conceived by Sebastian Krämer in 2017/2018, maintained and extended by David Plankensteiner between 2018 and 2021 and is currently maintained by Christoph Hotter and Laurin Ostermann [14].

As already mentioned, the framework is written in Julia. Julia is a script-like language that is similar to Python but has quite a large performance benefit over Python due to being JIT (just-in-time) compiled. This means that the execution time of Julia is similar to C and Fortran, whereas the execution time of Python and other languages used in scientific computing is often orders of magnitude slower than that (especially Python can be factors of 10^3 slower).

The toolbox was inspired by the Quantum Optics Toolbox for MATLAB [15] and the Python framework QuTiP [16]. Benchmarks for comparing QO.jl to the other two libraries can be found on the homepage of QO.jl.

3.2 Examples
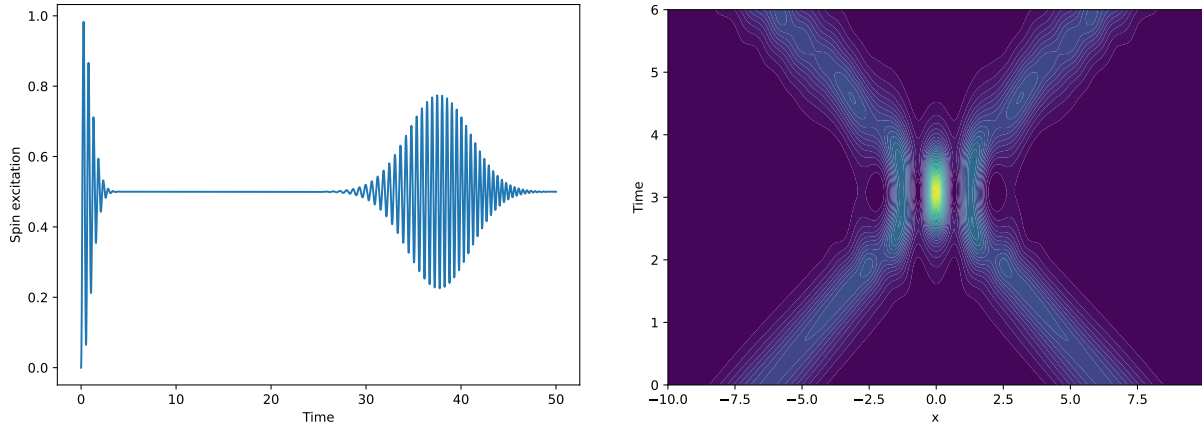
(a) Simulation of the Jaynes-Cummings System - the most important model in quantum optics.

(b) Simulation of the Gross-Pitaevskii equation for two colliding particles in 1D.

Figure 3.2: Two of the important examples given on the QO.jl homepage [14]

Various examples are given on the QO.jl homepage [14] that show what the framework can do and how easy it is to use. Figure 3.2 covers the most important example for quantum optics (figure 3.2a) and the most important example for this thesis (figure 3.2b). The Code for figure 3.2b can be seen in figure 3.3. With 24 lines of code (which also includes plotting through `matplotlib`), this is quite manageable. All you really have to do is create the basis, the Hamiltonian and the initial wave package. The toolbox does the rest.

QuantumOptics.jl is able to use various methods to simulate quantum systems. The exact method depends on the model and how the model is implemented. One of the most efficient methods and the method used for figure 3.3 and for the other calculations in this thesis is the split-operator method.

```
using QuantumOptics
b_x = PositionBasis(-10, 10, 300)
b_p = MomentumBasis(b_x)
Tpx = transform(b_p, b_x)
Txp = transform(b_x, b_p)
x = position(b_x)
p = momentum(b_p)

Hkin = LazyProduct(Txp, p^2/2, Tpx)
Hpsi = diagonaloperator(b_x, Ket(b_x).data)
H = LazySum(Hkin, Hpsi)

fquantum(t, ψ) = (Hpsi.data.nzval .= -50 .* abs2.(ψ.data); H)
ψₒ = gaussianstate(b_x,-2π,2,1.5) + gaussianstate(b_x,2π,-2,1.5)
normalize!(ψₒ)
tout, ψₜ = timeevolution.schroedinger_dynamic([0:0.01:6;], ψₒ, fquantum)
density = [abs2(ψ.data[j]) for ψ=ψₜ, j=1:length(b_x)]

using PyPlot
contourf(samplepoints(b_x),tout,density,50)
xlabel("x")
ylabel("Time")
tight_layout()
savefig("gross_pitaevskii.pdf")
```

Figure 3.3: The code for the simulation of the Gross-Pitaevskii equation as given on the QO.jl homepage.

3.3 Split-Operator method

As already mentioned in section 3.2, the split-operator method [17] is one of the most efficient methods in use by QO.jl. The basic derivation of the equation is quite simple (see [18] for reference): First, we split the Hamiltonian into position and momentum components ($H = H_r + H_k$) and enter this into the general ansatz for the time evolution of our wave function:

$$\psi(r, t + dt) = \exp\left(-\frac{iH\,dt}{\hbar}\right)\psi(r, t) = \exp\left(-\frac{i(H_r + H_k)\,dt}{\hbar}\right)\psi(r, t) \tag{3.1}$$

Then we apply the Baker–Campbell–Hausdorff formula [19][20] to the time evolution and get an approximation which is accurate up to d^2t:

$$\psi(r, t + dt) \approx \exp\left(-\frac{iH_r\,dt}{\hbar}\right)\exp\left(-\frac{iH_k\,dt}{\hbar}\right)\exp\left(-\frac{i[H_r,H_k]\,d^2t}{2\hbar}\right)\psi(r, t) + \mathcal{O}\left(d^2t\right) \tag{3.2}$$

This is not quite good enough. We also want to get rid of the commutator. Thus we apply strang splitting [21][20]:

$$\psi(r, t + dt) \approx \exp\left(-\frac{iH_r\,dt}{2\hbar}\right)\exp\left(-\frac{iH_k\,dt}{\hbar}\right)\exp\left(-\frac{iH_r\,dt}{2\hbar}\right)\psi(r, t) + \mathcal{O}\left(d^3t\right) \tag{3.3}$$

This reduces our error to d^3t. After that is done, we can apply Fourier transforms (FT) and inverse Fourier transforms (iFT) to directly get our time evolution:

$$\psi(r, t + dt) \approx \exp\left(-\frac{iH_r\,dt}{2\hbar}\right)\mathcal{F}^{-1}\left(\exp\left(-\frac{iH_k\,dt}{\hbar}\right)\mathcal{F}\left(\exp\left(-\frac{iH_r\,dt}{2\hbar}\psi(r, t)\right)\right)\right) + \mathcal{O}\left(d^3t\right) \tag{3.4}$$

This is the crucial step in this method: The components of the Hamiltonian are now always in the same space as the wave function (since we transform the wave function using FT/iFT). Numerically speaking this means that the operators in their respective basis are always diagonal. This means that if we apply the components of the Hamiltonian onto the wave function, we only need to do multiplications. And multiplications only require very little calculation time. The only other thing that we have to do besides the multiplications is Fourier transforms and inverse Fourier transforms, which are also quite fast, as the name suggests, if fast Fourier transform (FFT) is used.

That's it. Nothing more to do. Just multiplications and FFT (one of the oldest, fastest and most common algorithms in algorithm history). This is why this method is so efficient. Other methods often require various different methods of numerical calculation, including discrete integrals which usually demand quite a lot of calculation time while not even providing accurate results in many cases. The Euler method for example, while easy to implement, requires a lot of calculation time and usually does not the conserve energy of the system, making it physically very imprecise.

4 Results

This chapter covers the results of various simulations using QuantumOptics.jl and the split-operator method. Most sections cover a comparison between two parameter values to demonstrate the effect of the parameter on the probability density. However, due to the limited space available, only a few frames of the rendered video can be shown which additionally have to be quite small. It is therefore recommended to watch the associated video provided here [22]. The code used to generate these videos is documented here [23].

4.1 Basic simulation parameters and general remarks

(a) Simulation of frame 0. **(b)** Simulation of frame 20. **(c)** Simulation of frame 35.

(d) Simulation of frame 60. **(e)** Simulation of frame 75. **(f)** Simulation of frame 105.
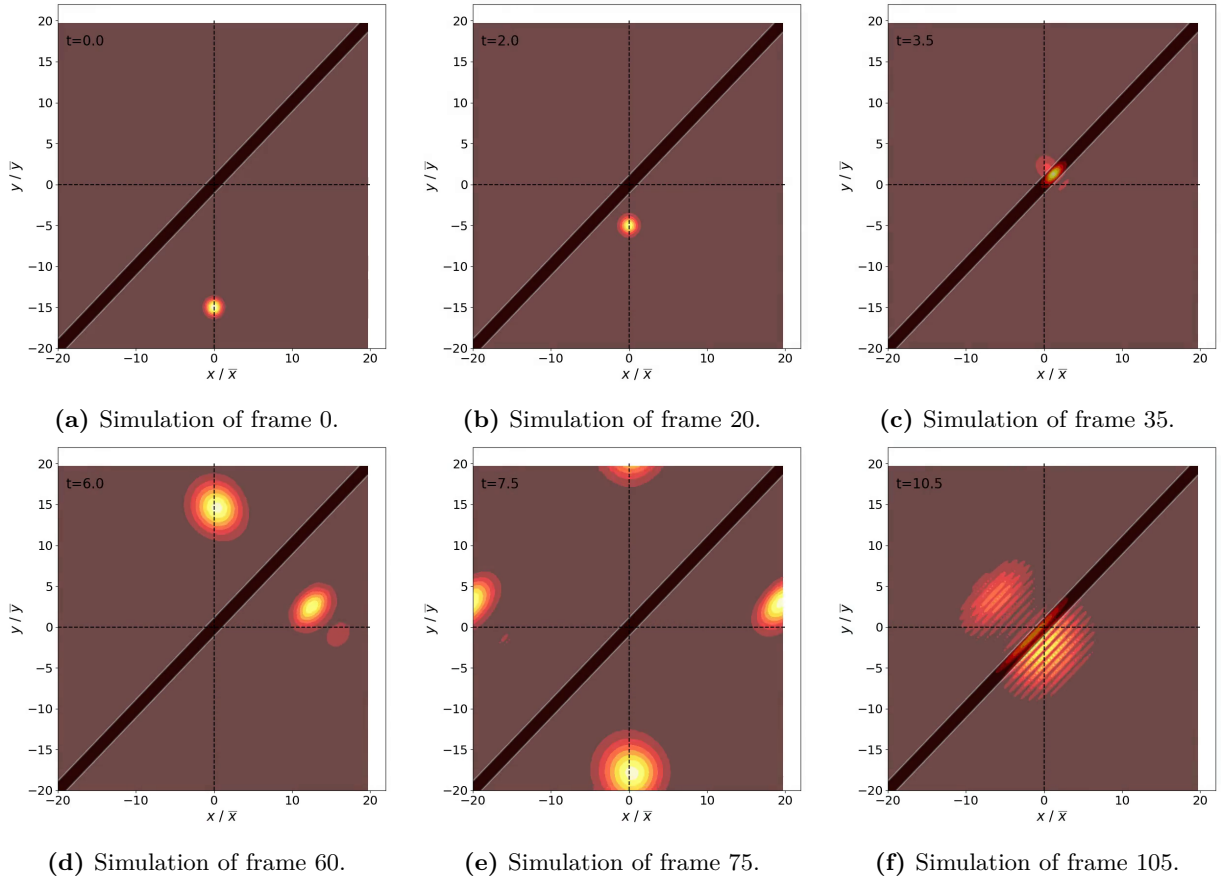
Figure 4.1: Simulation of the probability density for the basic parameters of the beam splitter.

Figure 4.1 shows the simulation that acts as a base for all the following simulations. The parameters for this are $g = -50\,\bar{m}\bar{x}^4\bar{t}^{-2}$ (the coefficient of the pseudopotential), $\alpha = 45°$ (the angle of

14

the potential), $V_B = 5.0\,\bar{m}\bar{x}^2\bar{t}^{-2}$ (the height of the potential barrier), $w = \pm1.0\,\bar{x}$ (the padding for the potential around the diagonal), $m = 1\,\bar{m}$ (the mass of the particle), $N = 128$ (the amount of discrete points along each axis and therefore the simulated states per axis - $128 \cdot 128 = 16\,384$ states in total), $v_0 = 5.0\,\bar{x}\bar{t}^{-1}$, $\Delta t = 0.1\,\bar{t}$ (the time step for the simulation), $t_{end} = 20.0\,\bar{t}$ (the end of the time span created for the simulation) and as particle type a gaussian particle (see section 2.2.3 for reference). All values are given in natural units (all constants set to 1). In addition to each of the base wave functions, a term $\exp(imv_0(x - x_0/2))$ was used to control the velocity/momentum of the particle. Each of the following simulations will use these as a base and modify one or more of them to demonstrate certain behavior of the system.

Another remark for all upcoming simulations is that the position base is set to be periodic. This means that if the wave function leaves the simulation area on one side, it will reappear on the other side. This can be seen between frames 60, 75 and 105 where the split particles leave the area on one side, reappear on the other side and then interfere with each other as they move closer to the potential barrier again (this can be better observed through the videos).

As already indicated, the beam splitting does indeed work with a rough 50:50 split. This was achieved by changing the value of V_B until it seemed to approach a 50:50 visually. This can be observed between frames 20, 35 and 60 where the particle hits the barrier and gets split into two parts. Interestingly though, the wave function seems to stay within the potential barrier for a few frames while sliding up the barrier (this can be observed in the videos) and distributing its content to both sides, vanishing at frame 60. The two split parts now continue independently. This leads to a slight offset from the center line of the transmitted part of the wave and a substantial offset of the reflected part. The larger offset of the reflected part can possibly be explained due to the reflection taking part at each potential edge. This leads to two reflected wave functions that overlap and due to the pseudopotential then merge into one wave function (more on that in section 4.5). This also leads to a slightly elongated wave function of the reflected part as can be observed in frames 60, 75 and 105. That is not the case for the transmitted part, which seems to keep its circular (2D Gaussian) waveform.

Another interesting aspect of this simulation is the value of g. The attractive pseudopotential shown in section 2.2.4 only had a coefficient $g = -1\,\bar{m}\bar{x}^4\bar{t}^{-2}$, but the g-factor used for the simulation is much stronger than that with $g = -50\,\bar{m}\bar{x}^4\bar{t}^{-2}$. This is required for the particle to stay together. For lower values, the natural dispersion becomes stronger than the pseudopotential, which leads to an increasing wave package (more on that in section 4.2). The value of g that is required for the particle to keep its form is also strongly dependent on the number of simulated states N of the system. The value had to be much bigger for higher precision calculations (more on that in section 4.8).

As already indicated, the interference patterns in frame 105 are to be expected. These come from the interactions of the transmitted part of each of the split waves with the part of the other wave that has not yet reached the potential or has already been reflected. Similar patterns can be seen on 90° reflections on potential barriers (e.g. the GIF [24] on the German Wikipedia page on the tunnel effect [25]).
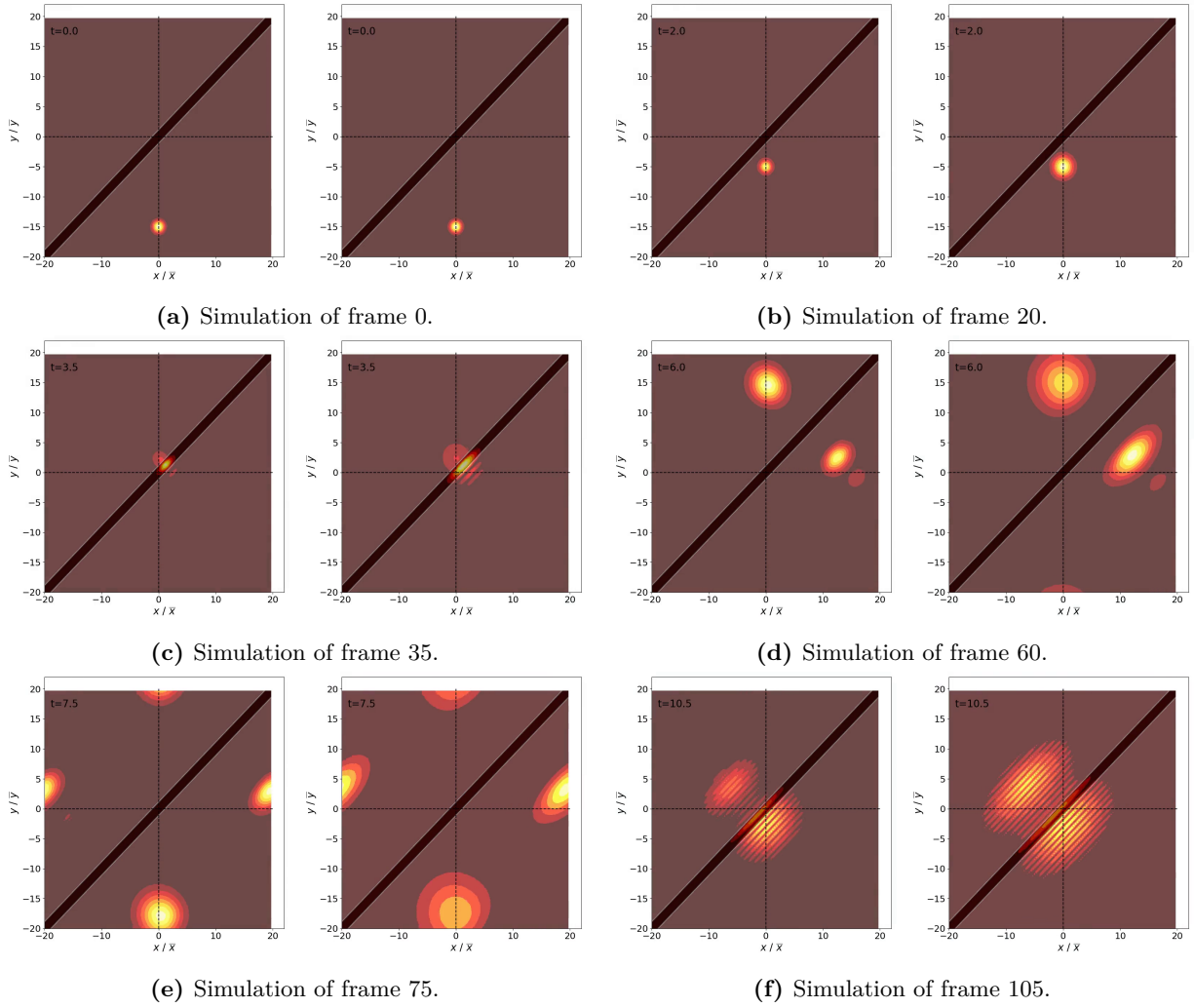
4.2 Strong vs. weak pseudopotential

(a) Simulation of frame 0.

(b) Simulation of frame 20.

(c) Simulation of frame 35.

(d) Simulation of frame 60.

(e) Simulation of frame 75.

(f) Simulation of frame 105.

Figure 4.2: Simulation of the probability density for a strong pseudopotential ($g = -50\,\bar{m}\bar{x}^4\bar{t}^{-2}$) on the left of each sub-figure vs a weaker potential ($g = -25\,\bar{m}\bar{x}^4\bar{t}^{-2}$) on the right.

Figure 4.2 shows the effect of a *g*-factor that is too small for the particle to stay together in comparison to the base parameter. Higher *g*-factors are unfortunately not possible to simulate because the particle then starts to collapse to a single point. The simulation then either doesn't continue or creates a rapidly expanding wave function. This rapid expansion can be observed in experiments and is called Bosenova. [26]

Due to the *g*-factor being too low, the wave function for $g = -25\,\bar{m}\bar{x}^4\bar{t}^{-2}$ starts to expand between frame 0 and frame 20 already. This accelerates after the split, so at frame 60, at which point the wave function for the stronger pseudopotential also starts to expand. This is due to the split of the waves and the associated decrease in amplitude of each part (the norm of the split waves combined has to be the same as of the initial wave). This also leads to a decrease in strength of the pseudopotential. So if the pseudopotential was strong enough to keep the particle at a certain size before the potential barrier, then it will be too weak after it.
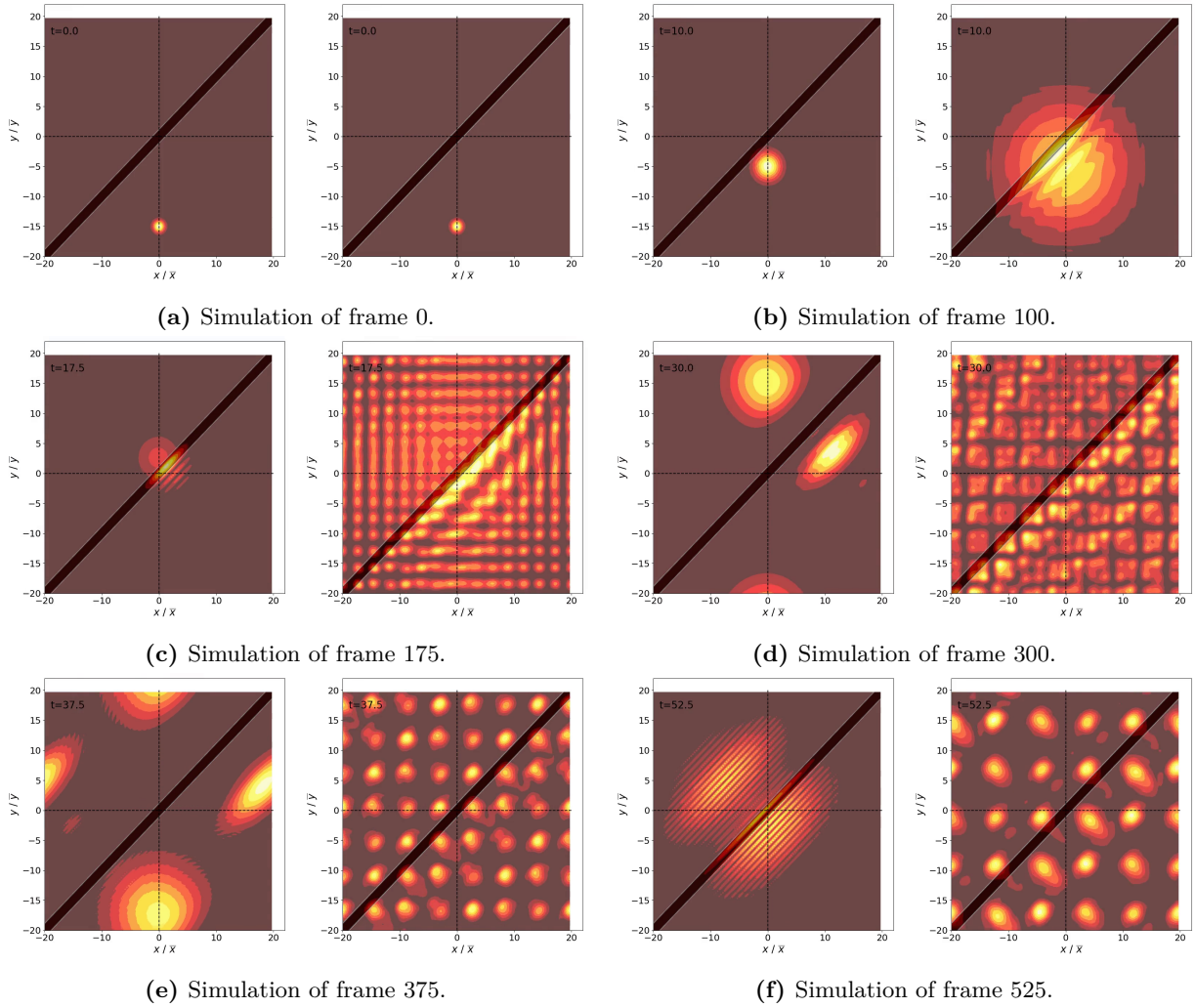
4.3 Heavy particle approximation

(a) Simulation of frame 0.

(b) Simulation of frame 100.

(c) Simulation of frame 175.

(d) Simulation of frame 300.

(e) Simulation of frame 375.

(f) Simulation of frame 525.

Figure 4.3: Simulation of the probability density for a regular particle with high mass ($m = 5\,\bar{m}$, $V_{\text{B}} = 0.9\,\bar{m}\bar{x}^2\bar{t}^{-2}$) on the left of each sub-figure and low mass ($m = 1\,\bar{m}$, $V_{\text{B}} = 0.2\,\bar{m}\bar{x}^2\bar{t}^{-2}$) on the right. The initial velocity of the particle was decreased to $v_0 = 1\,\bar{x}\bar{t}^{-1}$ and the simulation end time increased accordingly to $t_{\text{end}} = 100.0\,\bar{t}$. This was necessary because the momentum base is periodic. A momentum $p_0 = 10.0\,\bar{m}\bar{x}\bar{t}^{-1}$ would lead to backwards movement, $p_0 = 25.0\,\bar{m}\bar{x}\bar{t}^{-1}$ would lead to slow forward movement.

Figure 4.3 shows the heavy mass approximation for a heavy and a light particle. The heavy particle behaves similarly to the case with a weak *g*-factor with an even higher expansion rate, which could probably be further reduced to the same rate as for $g = -25\,\bar{m}\bar{x}^4\bar{t}^{-2}$. However, the light particle produces a somewhat unexpected result. The expansion is so fast that the particle approaches the size of the simulation area in frame 100 already. This leads to small circular wave packages that seem to periodically shift in size due to the continued expansion. This can again be better observed in the videos. This "fast" expansion rate is due to the reduction in v_0 compared to the base parameters which is not compensated for with a higher mass (see equation 2.18).
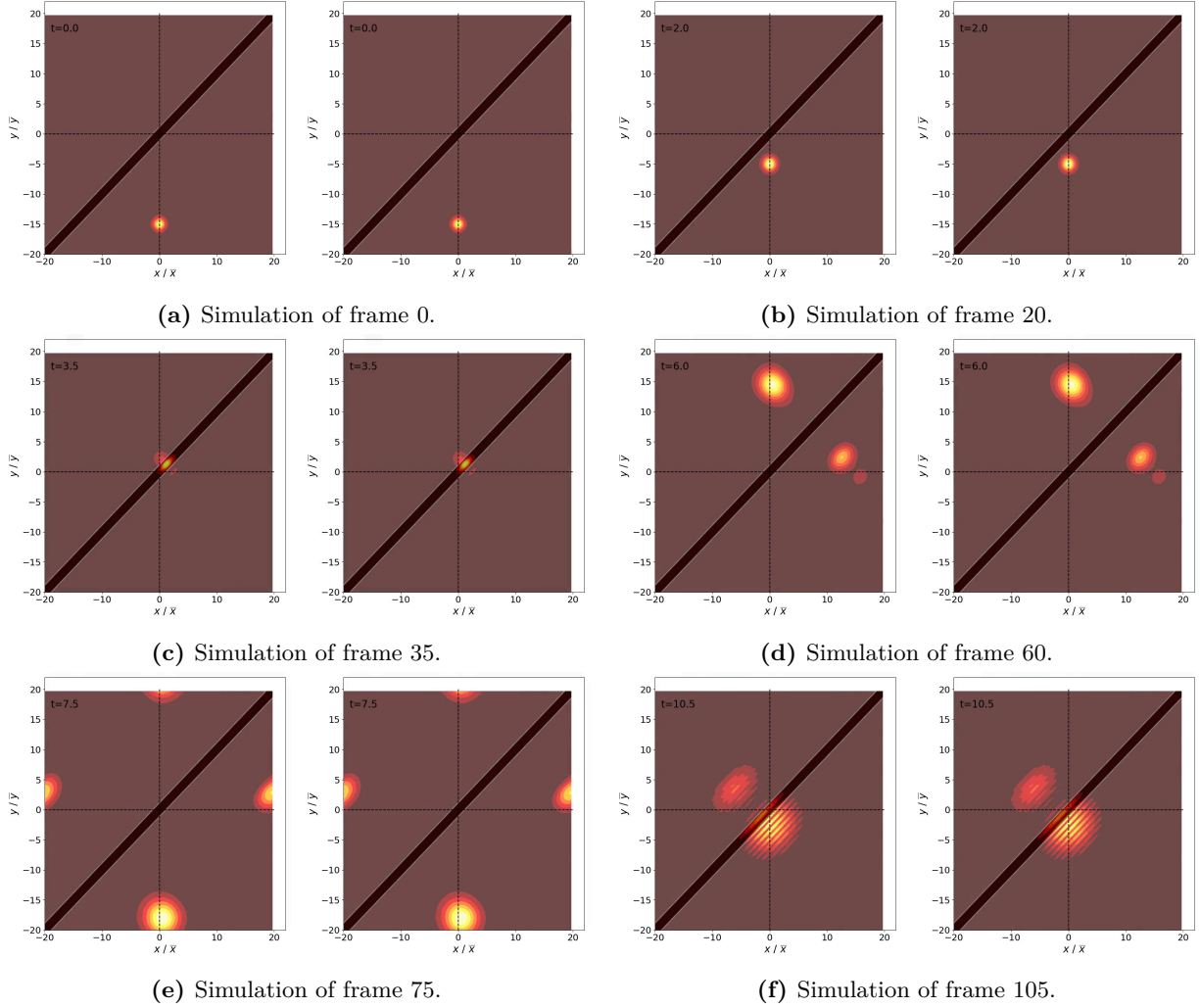
4.4 Different Soliton models in comparison

(a) Simulation of frame 0.

(b) Simulation of frame 20.

(c) Simulation of frame 35.

(d) Simulation of frame 60.

(e) Simulation of frame 75.

(f) Simulation of frame 105.

Figure 4.4: Simulation of the probability density for a bright soliton $\mathrm{sech}(x)$ on the left of each sub-figure and an inverted dark soliton $\sqrt{1 - \tanh^2(x)}$ on the right for $g = -50\,\bar{m}\bar{x}^4\bar{t}^{-2}$.

Figure 4.4 compares the two different soliton solutions to each other. Each 2D wave was built by multiplying a 1D wave for each axis together. The dark soliton solution was inverted in order to make it comparable to the other simulations. As already mentioned for the base parameters, each wave function was multiplied by $\exp(imv_0(x - x_0/2))$ to account for the momentum of the particle (once for each axis).

No real difference can be observed visually. Neither between these two nor in comparison to the Gaussian wave. The only exception being the amplitude of the reflected parts, which could also be due to a slightly different size of the initial wave packages.
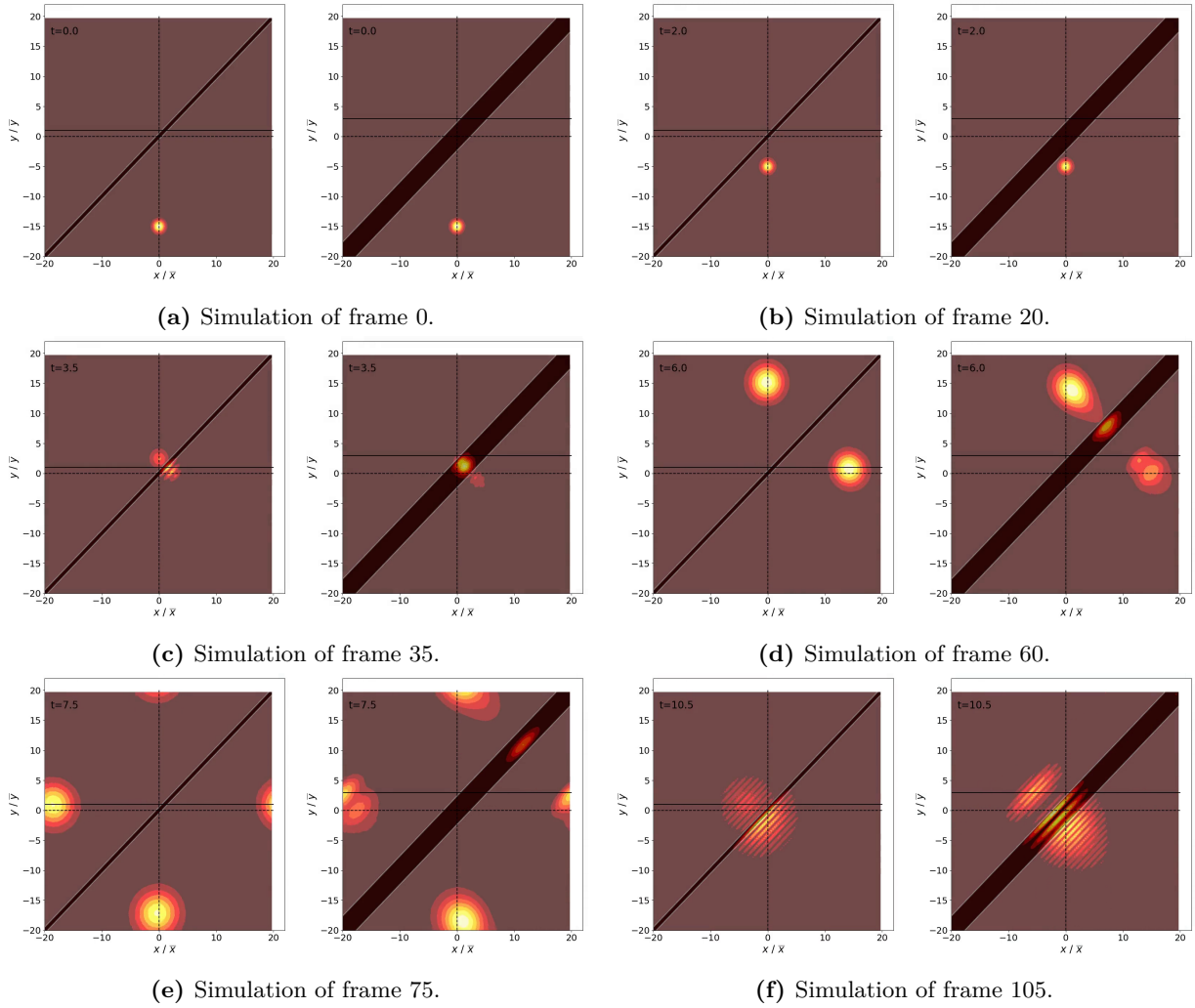
4.5 Wide vs. thin potential barrier

(a) Simulation of frame 0.

(b) Simulation of frame 20.

(c) Simulation of frame 35.

(d) Simulation of frame 60.

(e) Simulation of frame 75.

(f) Simulation of frame 105.

Figure 4.5: Simulation of the probability density for a narrow potential ($w = \pm 0.5\,\bar{x}$, $V_\mathrm{B} = 5.5\,\bar{m}\bar{x}^2\bar{t}^{-2}$) on the left of each sub-figure and a wide potential ($w = \pm 2.2\,\bar{x}$, $V_\mathrm{B} = 5.0\,\bar{m}\bar{x}^2\bar{t}^{-2}$) on the right.

Figure 4.5 compares two potentials with different widths in order to demonstrate the differences in reflection behavior. As observable in frame 60, the narrow potential produces a nearly perfectly circular reflected wave nearly without any offset to the center line. On the other hand, the two reflected parts of the wave of the wide potential seem to be so far separated from one another that the wave functions don't merge up as with the base parameters. The offset from the center line seems to be pretty much the same as for the base parameters. Interestingly, the strength of the potential V_B requires only a very minuscule increase for the narrow potential compared to the base parameters despite the width w being halved. The wide potential didn't require any adjustments of the potential height. Another interesting effect of the narrow potential is the destructive interference of the waves from frame 105 onward. The waves had the same intensity in frame 75, but start to interfere destructively in frame 105 which leads to a decrease in amplitude

19

for the horizontally moving wave that eventually leads to complete destruction (see the video for details).

4.6 Repulsive potential

(a) Simulation of frame 0.

(b) Simulation of frame 20.

(c) Simulation of frame 35.

(d) Simulation of frame 60.

(e) Simulation of frame 75.
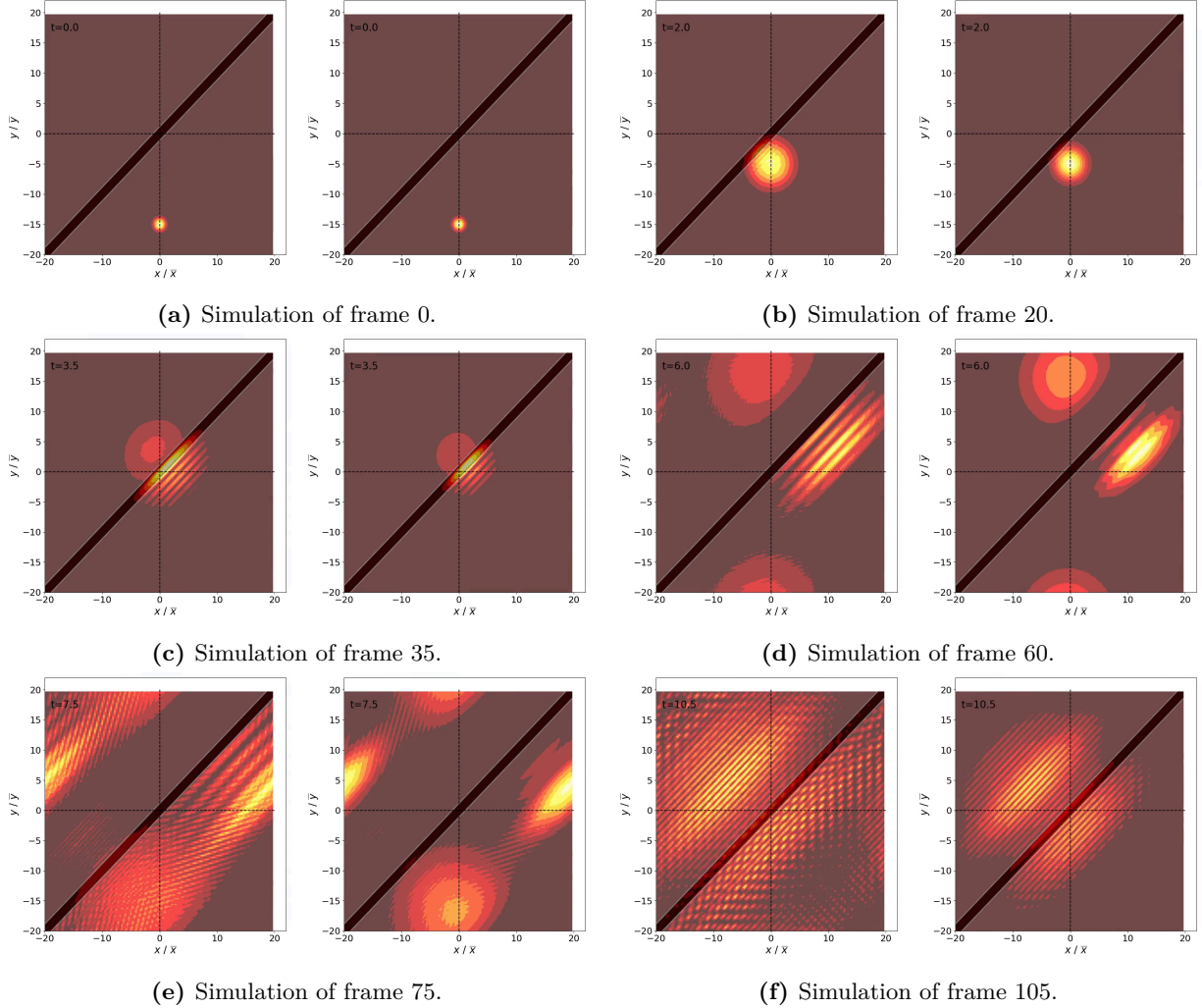
(f) Simulation of frame 105.

Figure 4.6: Simulation of the probability density for $g = 100\,\bar{m}\bar{x}^4\bar{t}^{-2}$ on the left of each sub-figure and $g = 25\,\bar{m}\bar{x}^4\bar{t}^{-2}$ on the right.

Figure 4.6 shows the effect of positive values for g on the wave function. As mentioned in section 2.2.4, a positive g-factor results in a repulsive potential, increasing the effect of the natural dispersion instead of decreasing it. An increase in wave size from lower g to higher g can already be observed in frame 20 and is only increasing from frame 20 onward. Due to the strong repulsive forces for $g = 100\,\bar{m}\bar{x}^4\bar{t}^{-2}$, the wave seems to scatter into many small dots towards the end of the simulation. This seems to be due to the interactions of the reflected wave with the transmitted wave in frame 75, which is only possible since the waves are large enough at this point to interact that way. For $g = 25\,\bar{m}\bar{x}^4\bar{t}^{-2}$ there also seems to be a weak interaction in frame 75, but not

enough to cause a major split of the wave, as can be seen in frame 105.
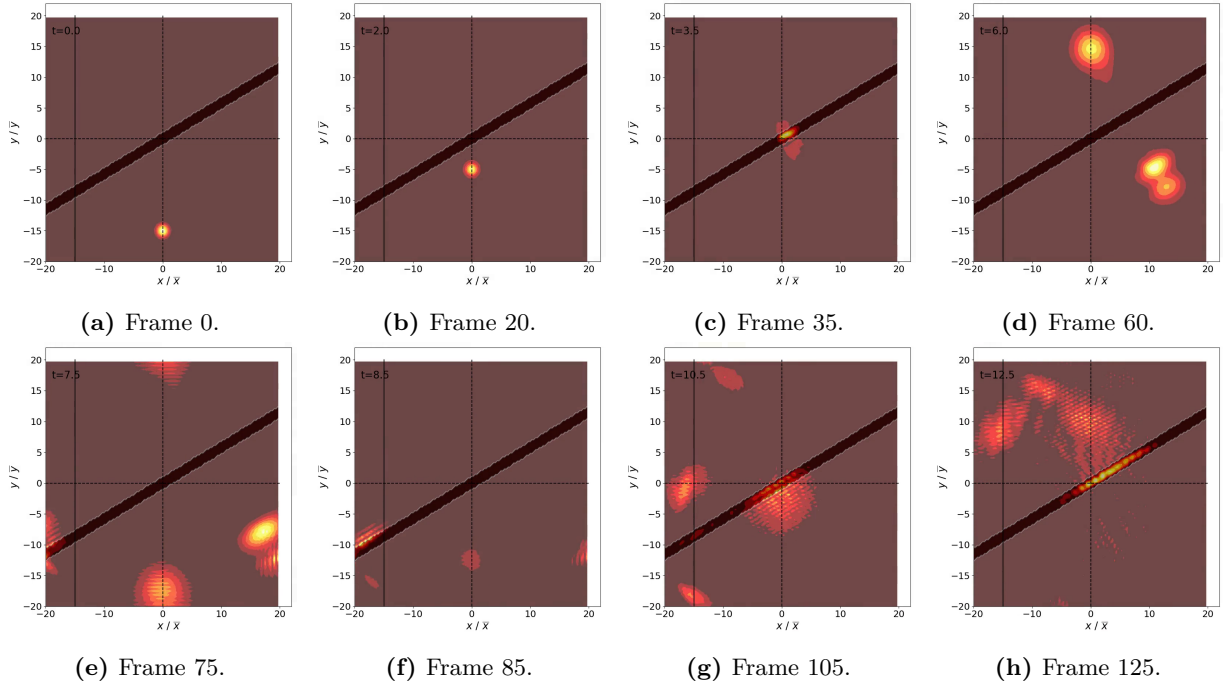
4.7 Lower angle potential

(a) Frame 0.   (b) Frame 20.   (c) Frame 35.   (d) Frame 60.

(e) Frame 75.   (f) Frame 85.   (g) Frame 105.   (h) Frame 125.

Figure 4.7: Simulation of the probability density for a potential $V_\mathrm{B} = 8.5\,\bar{m}\bar{x}^2\bar{t}^{-2}$ at an angle $\alpha = 30°$.

Figure 4.7 shows a potential at a reduced angle. The potential appears quite jagged with this setting. This is due to the fact that only $N = 128$ states could be simulated per axis with $16\,\mathrm{GiB}$ of memory, therefore causing serious discretization errors for lower angles. These discretization errors are then causing major scattering behavior of the waves, especially after the second reflection.

As expected, the wave gets reflected away from the horizontal axis at a certain angle in frame 60. To now investigate whether the law of reflection ("the angle of incidence equals the angle of reflection") also holds true for reflections on a potential barrier, one can investigate frames 75, 85, 105 and 125. This is when the reflected wave hits the potential barrier a second time and thus gets reflected a second time. The law of reflection now implies that the angle after the second reflection has to be the same as the original angle of incidence. This can especially be seen between frames 105 and 125 where the particle moves vertically along the helper line at $x = -15.0\,\bar{x}$.

The reflected wave seems to have a similar form as for the wide potential in section 4.5 where the two reflections at each edge cause two non-converging parts of the wave to form. But compared to the wide potential, the wave function for the angled reflection seems to be distorted and not really circular if you have a closer look at frame 60. This is probably again due to the jagged potential.

4.8 High precision calculation

(a) Simulation of frame 0.

(b) Simulation of frame 20.

(c) Simulation of frame 35.

(d) Simulation of frame 60.

(e) Simulation of frame 75.

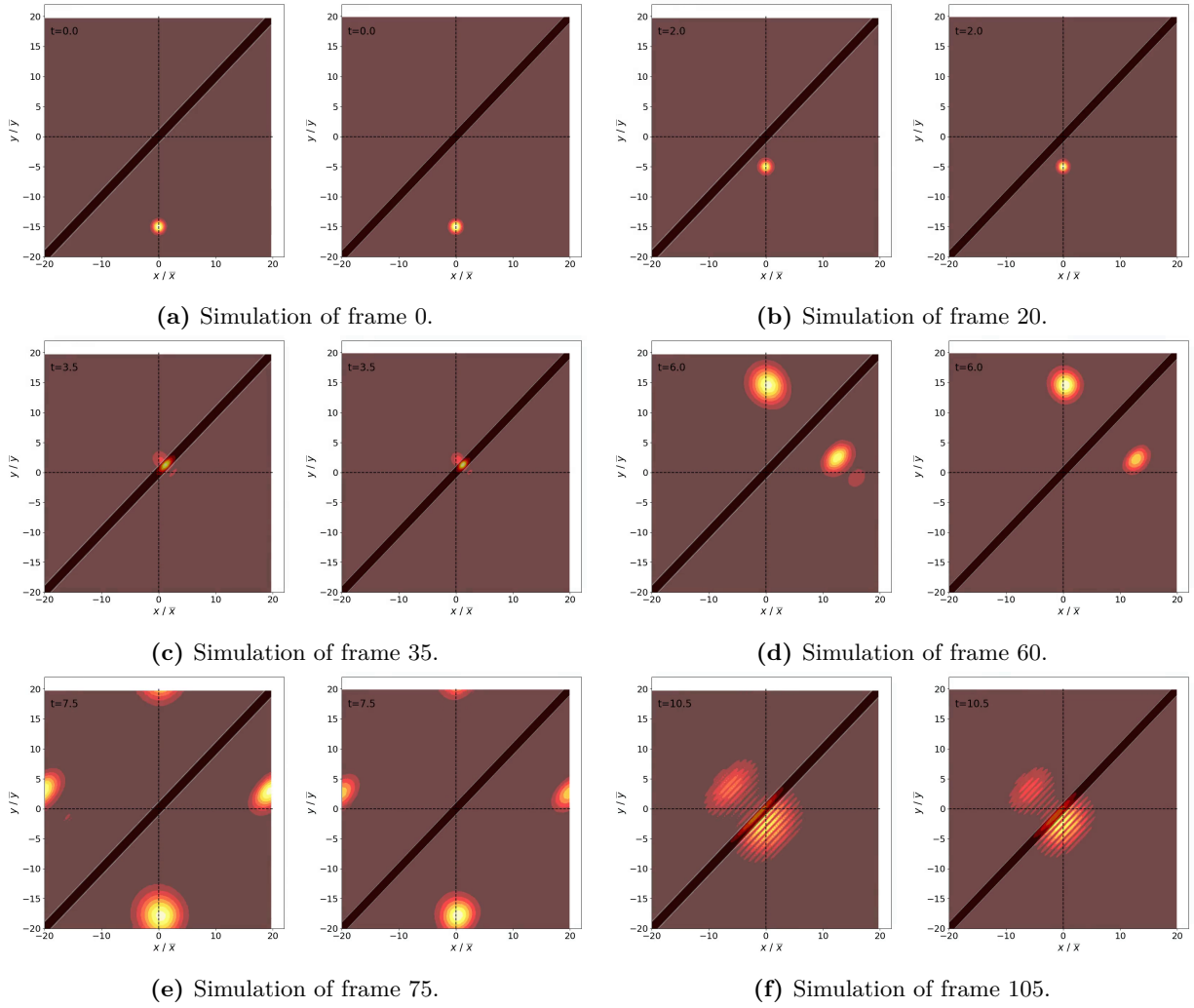**(f)** Simulation of frame 105.

Figure 4.8: Simulation of the probability density for the base parameters on the left of each sub-figure vs the higher precision calculation ($N = 384$, $g = -500\,\bar{m}\bar{x}^4\bar{t}^{-2}$) on the right.

Figure 4.8 shows the comparison of the base parameters with the associated higher precision calculation. There are no real obvious differences observable except for a slight reduction in amplitude for the higher precision calculation in frame 60.

The most interesting part about this simulation is that the *g*-factor had to be much higher than for the lower precision calculation. The reasons for this are not very clear, but it's probably due to the Fourier transform. A lower precision could cause major deviations after the Fourier transforms that could lead to a smaller effective pseudopotential. But this is basically just speculation.

Figure 4.9 is more interesting in this case. It shows the same comparison but for the case of a lower angle as in section 4.7. While not much different, the potential appears a lot less jagged and there also seems to be less scattering as expected. This is despite the fact that the simulation had to be run with $N = 384$ for $512\,\mathrm{GiB}$ of memory, which is not a power of 2 as required by most FFT algorithms. Simulations with $N = 512$ would run into `OutOfMemoryError()` and $N = 256$

was not a real improvement over $N = 128$. Simulations with $N = 400$ would cause even more scattering due to the strong deviation from powers of 2. Therefore, $N = 384$ was chosen as a compromise.
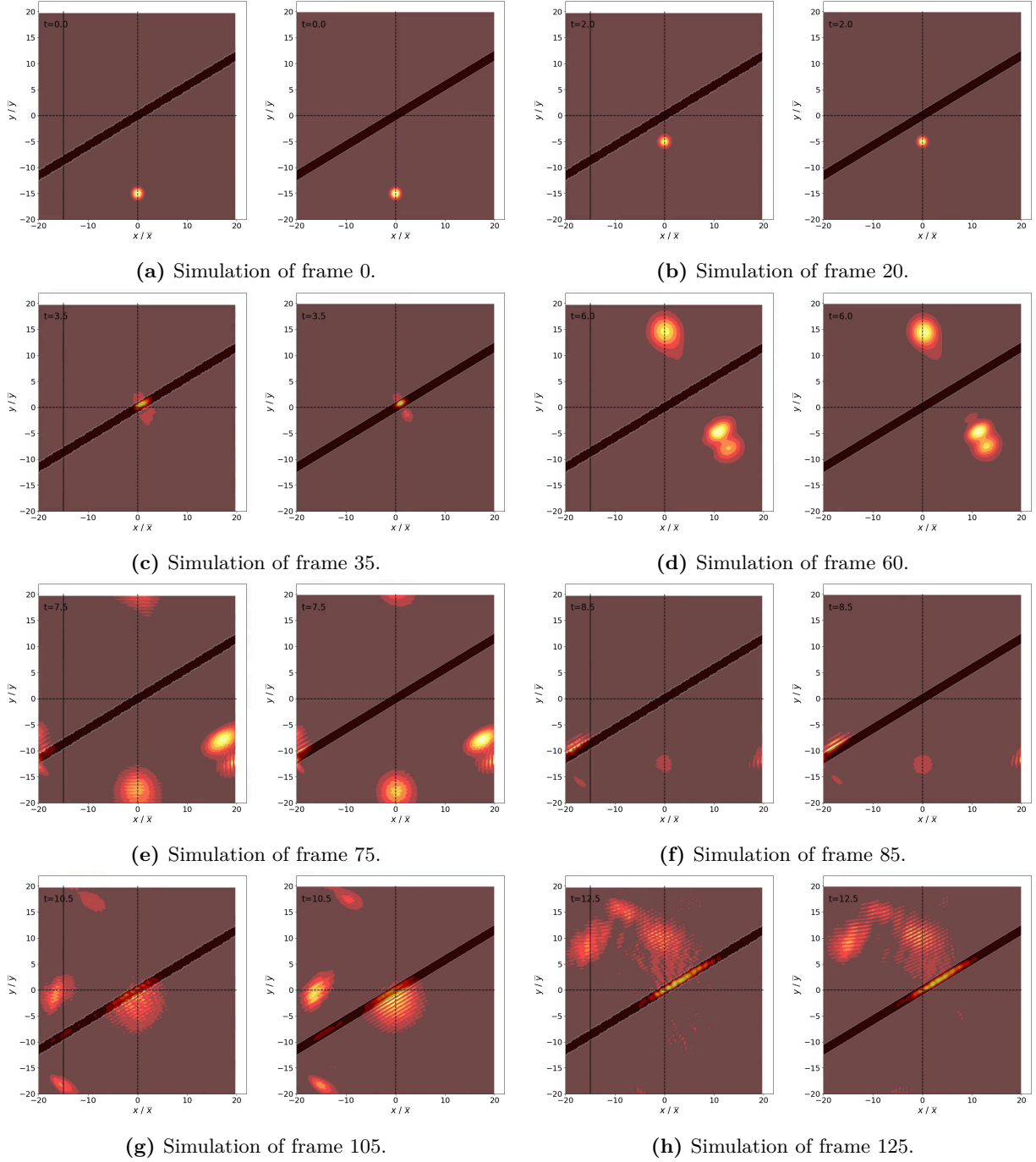

(a) Simulation of frame 0.

(b) Simulation of frame 20.

(c) Simulation of frame 35.

(d) Simulation of frame 60.

(e) Simulation of frame 75.

(f) Simulation of frame 85.

(g) Simulation of frame 105.

(h) Simulation of frame 125.

Figure 4.9: Simulation of the probability density for the lower angled setting ($V_{\mathrm{B}} = 8.5\,\bar{m}\bar{x}^2\bar{t}^{-2}$, $\alpha = 30°$) from fig. 4.7 on the left of each sub-figure vs the higher precision calculation for the lower angle ($V_{\mathrm{B}} = 8.5\,\bar{m}\bar{x}^2\bar{t}^{-2}$, $\alpha = 30°$, $N = 384$, $g = -500\,\bar{m}\bar{x}^4\bar{t}^{-2}$) on the right.

5 Conclusion

Various predictions were successfully confirmed in this thesis. The split of the BEC into two wave packages, being the most important aspect of this thesis, has been successfully demonstrated. Even second and third reflections/transmissions were observable. The effect of the pseudopotential in reducing or even negating the natural dispersion of the wave package was shown as well as the approximation with a heavy particle. The Gaussian wave package was confirmed to be a good approximation to the two soliton solutions, which didn't seem to differ significantly from one another. The change in reflection behavior with different potential widths w confirmed the suspicions about the reflections at each potential edge. A positive g-factor led to an increased expansion rate of the BEC due to the now repulsive pseudopotential as expected. The law of reflection ("the angle of incidence equals the angle of reflection") was also demonstrated to hold true for BEC reflections on a potential barrier.

But there were also some unexpected results and some issues demonstrated in simulating the splitting of a BEC. The most important problem is the expansion of the particle after the reflection/transmission due to the reduction in amplitude and the inability to further increase the g-factor to counter this. A possible workaround for this could be to start with two particles and then have them move in such a way that their transmitted/reflected part overlap each other. The resulting waves should then have the same amplitude as the initial wave, which should result in both particles retaining their size after colliding with the barrier.

Another problem is the jagged potential for lower angles as well as the scattering that happens after a certain point. The solution to both of these issues would be to increase the resolution of the simulation. This is however not possible due to memory restrictions. Some optimization in the code might be possible, but running the simulation with $N = 512$ would probably still require more than $512\,\mathrm{GiB}$ of memory. An even better resolution with $N = 1024$ would probably require a memory size close to $16\,\mathrm{TiB}$, which is not possible on an ordinary motherboard.

Unexpected results where the field of periodically changing BECs that resulted from a low mass in section 4.3 as well as the minuscule amount of change in the strength of the potential barrier required for the narrow potential to keep a rough 50:50 split. The first one could probably be explained by a simple overlap of the expanding wave function. The reflected and transmitted parts then meet at certain points in the simulation area and cause these periodically changing wave packages. The second one seems to be a bit strange at first, but could probably be explained with a more detailed analysis. But this would go beyond the scope of this thesis.

References

[1] Angstrom Engineering, *Beam splitters*, `https://angstromengineering.com/applications/introduction-optical-coatings/beam-splitters` (visited on 2023-06-21).

[2] S. J. Kim, H. Yu, S. T. Gang, and J. B. Kim, "Matter-wave beam splitter on an atom chip for a portable atom interferometer", Applied Physics B **123**, 154, ISSN: 1432-0649 (2017) `10.1007/s00340-017-6719-6`.

[3] F. Schwabl, *Statistische mechanik*, ger (Springer, Secaucus, 2006), ISBN: 3540310959.

[4] Universität Innsbruck, *Quantum gas turns supersolid*, (2019) `https://www.uibk.ac.at/en/newsroom/2019/quantum-gas-turns-supersolid`.

[5] L. Sonderhouse, C. Sanner, R. B. Hutson, A. Goban, T. Bilitewski, L. Yan, W. R. Milner, A. M. Rey, and J. Ye, "Thermodynamics of a deeply degenerate SU(n)-symmetric fermi gas", Nature Physics **16**, 1216–1221 (2020) `10.1038/s41567-020-0986-6`.

[6] Wikimedia Commons, *Bose–einstein condensate*, File: `Bose Einstein condensate.png`, (1995) `https://commons.wikimedia.org/wiki/File:Bose_Einstein_condensate.png` (visited on 2023-06-20).

[7] Università di Padova, *Derivation of the gross-pitaevskii equation and applications*, (2019) `https://materia.dfa.unipd.it/salasnich/talk-patna19b.pdf` (visited on 2023-06-22).

[8] C. W. Gardiner and P. Zoller, *The quantum world of ultra-cold atoms and light.: (ultra-cold atoms)*, eng, Vol. 5, Cold atoms (World Scientific Publishing Europe Ltd, 2017), ISBN: 9781786344175, `10.1142/9781786344182`.

[9] E. Weisstein, *Delta function*, `https://mathworld.wolfram.com/DeltaFunction.html` (visited on 2023-07-28).

[10] P. Drazin and R. Johnson, *Solitons: an introduction*, Cambridge Texts in Applied Mathematics (Cambridge University Press, 1989), ISBN: 9780521336550.

[11] Università di Padova, *Bright and dark solitons of the gross-pitaevskii equation*, (2020) `https://materia.dfa.unipd.it/salasnich/phd/phd2020-solitons.pdf` (visited on 2023-06-23).

[12] M. Schwartz, *Lecture 11: wavepackets and dispersion*, `https://scholar.harvard.edu/files/schwartz/files/lecture11-wavepackets.pdf` (visited on 2023-06-26).

[13] Wikimedia Commons, *Tunneleffekt*, File:`TunnelEffektKling1.png`, (2010) `https://commons.wikimedia.org/wiki/File:TunnelEffektKling1.png` (visited on 2023-06-30).

[14] CQED Group, Universität Innsbruck, *Quantumoptics.jl homepage*, `https://qojulia.org/` (visited on 2023-06-26).

References

[15] Quantum Optics Theory Group, University of Auckland, *Quantum optics toolbox for matlab*, `https://qo.phy.auckland.ac.nz/toolbox/` (visited on 2023-07-28).

[16] J. R. Johansson and P. D. Nation, *Quantum toolbox in python*, `https://qutip.org/` (visited on 2023-07-28).

[17] S. M. Greene and V. S. Batista, "Tensor-train split-operator fourier transform (tt-soft) method: multidimensional nonadiabatic quantum dynamics", Journal of Chemical Theory and Computation **13**, 4034–4042, ISSN: 1549-9618 (2017) `10.1021/acs.jctc.7b00608`.

[18] J. Schloss, *The split-operator method*, `https://www.algorithm-archive.org/contents/split-operator_method/split-operator_method.html` (visited on 2023-06-26).

[19] Department of Physics, Duke University, *Notes on baker-campbell-hausdorff (bch) formulae*, `http://webhome.phy.duke.edu/~mehen/760/ProblemSets/BCH.pdf` (visited on 2023-07-28).

[20] M. Brunner, "Local error analysis for generalised splitting methods.", en, `10.34726/HSS.2020.61061` (2020) `10.34726/HSS.2020.61061`.

[21] Numerical Analysis and Scientific Computing Group, Universität Innsbruck, *Lecture 10: operator splitting*, `https://www.uibk.ac.at/mathematik/na/isem/isem15_lecture10.pdf` (visited on 2023-07-28).

[22] M. A. Schöpf, "A beam splitter for interacting quantum particles - videos", `10.5281/zenodo.8194018` (2023) `10.5281/zenodo.8194018`.

[23] M. Schöpf, *DevNoteHQ/BEC-Beam-Splitter: Release for thesis submission*, version v1.0.0, 2023-07, `10.5281/zenodo.8194039`.

[24] Wikimedia Commons, *File:effettunnel.gif*, `https://commons.wikimedia.org/wiki/File:EffetTunnel.gif` (visited on 2023-07-28).

[25] Wikimedia Commons, *Tunneleffekt*, `https://de.wikipedia.org/wiki/Tunneleffekt` (visited on 2023-07-28).

[26] P. A. Altin, G. R. Dennis, G. D. McDonald, D. Döring, J. E. Debs, J. D. Close, C. M. Savage, and N. P. Robins, "Collapse and three-body loss in a ^{85}rb bose-einstein condensate", Phys. Rev. A **84**, 033632 (2011) `10.1103/PhysRevA.84.033632`.